submitted
8/6/07
JFC

Radiolytic Gas-Driven Cryovolcanism in the Outer Solar System

John F. Cooper[1], Paul D. Cooper[2], Edward C. Sittler[3], Steven J. Sturner[4,5], Abigail M. Rymer[6], and Matthew E. Hill[6]

[1]*Heliospheric Physics Laboratory, Code 672, NASA Goddard Space Flight Center, 8800 Greenbelt Road, Greenbelt, MD, 20771 USA*

[2]*Department of Chemistry and Biochemistry, MS 3E2, George Mason University, 4400 University Drive, Fairfax, VA, 22030 USA*

[3]*Geospace Physics Laboratory, Code 673, NASA Goddard Space Flight Center, Greenbelt, MD, 20771 USA*

[4]*CRESST and Astroparticle Physics Laboratory, Code 661, NASA Goddard Space Flight Center, Greenbelt, MD 20771, USA*

[5]*Universities Space Research Association, 10211 Wicopin Circle, Suite 500, Columbia, MD 21044, USA*

[6]*Applied Physics Laboratory, Johns Hopkins Laboratory, 11100 Johns Hopkins Road, Laurel, MD 20723-6005, USA*

submitted to Journal of Geophysical Research - Planets, August 6, 2007

Abstract

Water ices in surface crusts of Europa, Enceladus, Saturn's main rings, and Kuiper Belt Objects can become heavily oxidized from radiolytic chemical alteration of near-surface water ice by space environment irradiation. Oxidant accumulations and gas production are manifested in part through observed H_2O_2 on Europa. tentatively also on Enceladus, and found elsewhere in gaseous or condensed phases at moons and rings of Jupiter and Saturn. On subsequent chemical contact in sub-surface environments with significant concentrations of primordially abundant reductants such as NH_3 and CH_4, oxidants of radiolytic origin can react exothermically to power gas-driven cryovolcanism. The gas-piston effect enormously amplifies the mass flow output in the case of gas formation at basal thermal margins of incompressible fluid reservoirs. Surface irradiation, H_2O_2 production, NH_3 oxidation, and resultant heat, gas, and gas-driven mass flow rates are computed in the fluid reservoir case for selected bodies. At Enceladus the oxidant power inputs are comparable to limits on non-thermal kinetic power for the south polar plumes. Total heat output and plume gas abundance may be accounted for at Enceladus if plume activity is cyclic in high and low "Old Faithful" phases, so that oxidants can accumulate during low activity phases. Interior upwelling of primordially abundant NH_3 and CH_4 hydrates is assumed to resupply the reductant fuels. Much lower irradiation fluxes on Kuiper Belt Objects require correspondingly larger times for accumulation of oxidants to produce comparable resurfacing, but brightness and surface composition of some objects suggest that such activity may be ongoing.

Introduction

Explosive volcanism on Earth originates from gas-driven (mostly H_2O vapor and CO_2) ejection at high temperature of an incompressible fluid from a subsurface magma reservoir to the planetary surface. High temperatures and plume gas output from volcanic hot spots at Io suggest a similar propulsive process. Comet outgassing from solar heating on approach to the Sun is well known, presumably involving release of trapped gases from cometary ices. Outgassing of N_2 has previously been detected [*Soderblom et al.*, 1990] by Voyager 2 at Triton, the largest moon of Neptune, and appears to be similarly driven by solar heating [*Brown et al.*, 1990; *Kirk et al.*, 1990], but the presence of subsurface fluids is unknown. Charon now shows potential surface evidence in ammonia hydrates for cryovolcanic flows from the subsurface [*Cook et al.*, 2007]. Absence of any ongoing surface change on Europa [*Phillips et al.*, 2000] suggests lack in the surface-accessible ice crust environment of cryovolcanic energy sources. A thick ice crust would likely preclude direct access to Europa's surface of dissolved gases from a putative subsurface ocean indicated by surface geologic features and induced magnetic fields [*Pappalardo et al.*, 1999].

Dramatically visible ice plume activity at Enceladus [*Porco et al.*, 2006] now provides unique opportunities for investigation with repeated observations during the continuing Cassini mission at Saturn. The measured presence of H_2O, CH_4, simple hydrocarbons, and a yet-unresolved mixture of CO and N_2 [*Waite et al.*, 2006] in the plume gas may indicate cryovolcanism involving the liquid water reservoir inferred by *Porco et al.* [2006]. However, a comet-like process involving only heat-driven release of trapped gases from ice clathrates has also been suggested [*Kieffer et al.*, 2007]. Although NH_3 is not highly abundant in either the plume gas [*Waite et al.*, 2006] or in the surface ice [*Brown et al.*, 2006], high temperature chemistry at the deep core-mantle boundary has been proposed by *Matson et al.* [2006] as the gas and hydrocarbon source.

Here we propose an alternative process for production of volatile gases that could drive cryovolcanism on Enceladus and other icy bodies with irradiated near-surface water ices. This process arises from interaction of continuously produced radiolytic oxidants and primordial chemistry. First, the unique aspect of this model is that chemical energy for oxidation arises in the outer ice crusts of planetary bodies from the continuous irradiation of near-surface water ice by energetic charged particles from the magnetospheric, heliospheric, and local interstellar space environments. Second, chemical energy and cryovolcanic driver gases are released by oxidation of primordially abundant reduced "fuel" compounds including ammonia, methane, and other hydrocarbons that originally accreted with water ice to form the underlying low density ice mantles of these bodies. Gravitational tides, internal tectonic activity, and radioisotope decay provide internal heating to increase rates of oxidant-fuel chemical reactions in cryogenic ice environments. The high exothermic energy yields of these reactions can potentially make the reactions self-sustaining. The subsurface liquid reservoir advocated for Enceladus by *Porco et al.* [2006] would provide an ideal high thermal gradient environment around the ice-liquid margins of the reservoir to sustain such reactions. Since reaction rates would increase with temperature in the 80 – 273 K range expected at the margins of a high-temperature water reservoir, exothermic heat production would raise local temperatures at reaction sites, and the reactants may concentrate in these locations, explosive results might be expected as observed.

The primary oxidant, O_2, in Earth's atmosphere comes from biological photosynthesis, but surface oxidants on icy surfaces in the outer solar system are naturally produced in exposed water ice by radiolysis from irradiation by energetic charged particles and solar ultraviolet photons. Europa, Ganymede, and Saturn's rings all have atmospheric environments of molecular oxygen presumably arising from particle or photon irradiation [*Hall et al.*, 1995, 1998; *Johnson et al.*, 2006], while all three icy Galilean moons have condensed phase O_2 in the surface ice [*Spencer et al.*, 1995; *Spencer and Calvin*, 2002]. Ozone is a sensitive proxy for atmospheric oxygen and is detected at Ganymede [*Noll et al.*, 1996], as well as at the Saturn moons Dione and Rhea [*Noll et al.*, 1997]. Presence of oxidants may be indirectly indicated by detection of atmospheric CO_2 as a potential oxidation product at Callisto [*Carlson*, 1999] and of surface CO_2 at Europa [*McCord et al.*, 1998b], Ganymede [*Hibbitts et al.*, 2003], and Callisto [*Hibbitts et al.*, 2000, 2002]. Further Callisto spectral observations and associated models [*Strobel et al.*, 2002; *Liang et al.*, 2005] suggest that atmospheric O_2, CO_2, and CO may be even more abundant on Callisto than the CO_2 first reported by Carlson [1999]. Cassini spectral mapping measurements [*Buratti et al.*, 2005] show CO_2 in the ice-rich surface environment of the small outer moon Iapetus at Saturn. The present paper explores the possibility that N_2 and CO_2 in the Enceladus plume gas [*Waite et al.*, 2005] might arise as oxidation products of radiolytic processes.

The radiolytic oxidant of highest known yield, hydrogen peroxide (H_2O_2), is produced in low-temperature laboratory measurements [*Johnson et al.*, 2004; *Moore and Hudson*, 2000; *Gomis et al.*, 2004a, 2004b; *Loeffler et al.*, 2006a] at yields of $G = 0.1 - 0.4$ H_2O_2 molecules per 100 eV of ionisation energy deposited by incident primary charged particles. The measured yield depends on existing abundances of other oxidants and is highest in the presence of O_2 and CO_2 within the irradiated ice. Although present experimental yields for direct production of O_2 are highly uncertain [*Johnson et al.*, 2004] by orders of magnitude at $G = 10^{-4}$ to 10^{-1}, even slow accumulation over millions of years in volume ice could saturate the ice crusts of irradiated icy moons and ring bodies, while also boosting the H_2O_2 yield and cumulative concentrations. Sublimation of directly irradiated water ice can also concentrate the H_2O_2 product [*Loeffler et al.*, 2006a], potentially producing explosive [Andrews, 1990] heating and oxidation transients upon exothermic dissociation of the concentrated peroxide.

Hydrogen peroxide has been detected at the maximally high source rates on Europa's heavily irradiated surface with surface concentrations ~ 0.1% relative to water ice [*Carlson et al.*, 1999] and is possibly present as a UV-absorbing component in surface ices of Ganymede and Callisto [*Hendrix et al.*, 1999a, 1999b]. There are preliminary reports of detection via near-infrared absorption on Enceladus [*Newman et al.*, 2006, 2007]. The relatively short lifetimes (four days at Jupiter, twenty days at Saturn) for H_2O_2 dissociation by solar ultraviolet photons make surface detection difficult at sensible depths up to a few hundred micrometers. Products of more penetrating irradiation at millimeter to meter depths [*Cooper et al.*, 2001] beyond the UV penetration range ~0.15 μm [*Carlson et al.*, 1999] would, however, continue to accumulate. Furthermore, burial of radiation products by water frost deposition from cryovolcanic emissions may be faster than the production rate. Burial by meteoritic impact gardening may also protect radiolytic products from photolytic destruction as suggested earlier for Europa [*Cooper et al.*, 2001].

Low abundances of gaseous CH_4 in the atmospheres of Earth, and of Mars [*Formisano et al.*, 2004; *Mumma et al.*, 2004], illustrate that oxidants and reductants cannot long co-exist in chemically reactive environments where continuous sources must replenish the observed gas. The presence of abundant frozen CH_4 on Pluto, Eris, and other Kuiper Belt Objects [*Cruikshank et al.*, 1997; *Brown et al.*, 2005], and of atmospheric CH_4 on Titan [*Niemann et al.*, 2005], indicates that oxidized water ices are not presently in direct chemical contact with the sensible surfaces and atmospheres of these bodies. However, the CH_4 surface layers on icy bodies, and the dominant CH_4 hydrocarbon in Titan's atmosphere, could be ejecta from past and even ongoing cryovolcanism, as arising from occasional interactions of otherwise segregated oxidant and reductant concentrations in the near-surface environment.

Fluid environments are thought to be essential for evolution of life but also enable the dramatic effects of gas-driven volcanism by the combined gas-piston interaction of subsurface fluids and gases. Liquid water oceans at tens to hundreds of kilometres in depth may account for induced magnetic field measurements at the icy Galilean moons of Jupiter [*Kivelson et al.*, 2004], and a south polar water reservoir may account in part for the plume activity at Enceladus. Other internal heat sources, e.g. radioisotope decay, may account for modern presence of fluids even in cases of weak tidal heating, as at Callisto [*McKinnon*, 2006; *McKinnon and Barr*, 2006]. If so, even the icy dwarf planets of the Kuiper Belt, many much larger than Enceladus, might have subsurface reservoirs of the requisite incompressible fluids at eutectic temperatures, e.g. 173 K for H_2O-NH_3 mixtures, to enable active cryovolcanism.

In this paper we quantitatively model radiolytic gas-driven cryovolcanism for illustrative cases of Enceladus and elsewhere in terms of the proposed sequence of radiolytic chemical processes from surface irradiation and oxidant production, to exothermic H_2O_2 dissociation and fuel oxidation, and finally to gas production giving rise to plume emissions. Underlying assumptions in the model are vertical mobility of radiolytic products and underlying fuel compounds in the south polar ice crust, trace abundances of metal catalysts to trigger H_2O_2 dissociation even at low temperatures, an unlimited supply of fuel compounds presumably brought up by rheological flows from deep primordial reservoirs, and a subsurface H_2O fluid reservoir that underlies the polar cap. The fluid reservoir provides a steep thermal gradient around its warm ice margins to accelerate exothermic chemical reactions, becomes pressurized with gaseous oxidation products, and provides the bulk of plume mass flow through gas-driven propulsion of the incompressible fluid. Using representative flux spectra for electron or proton irradiation in selected orbital environments of the outer solar system, we compute the radiolytic model parameters for icy bodies in these environments under the above common assumptions to show the full potential range of cryovolcanism that could be driven by radiolytic gases in diverse outer planet environments from Europa and Enceladus to the Kuiper Belt and the Oort Cloud. In the final discussion we then characterize the strengths and weaknesses of this model with respect to those of other models previously published and widely reported for Enceladus.

Enceladus

The water ice [*Porco et al.*, 2006], neutral gas [*Waite et al.*, 2006], and dust [*Spahn et al.*, 2006] plumes of Enceladus provide the second known example of active cryovolcanism and are also produced, like on Triton, in an icy surface heavily irradiated by energetic particles, mostly electrons, in the orbital environment of a planetary magnetosphere. We suggest that the plume activity at Enceladus could at least partly arise from sporadic interactions of radiolytic oxidants and primordially abundant reductants brought into direct chemical contact within the near-surface (tens of meters to kilometers) environment by internal rheologic processes. Volatile gas products of such reactions, and the primary drivers for cryovolcanic activity, could include CO_2 and CO, commonly found in outgassing from comets, from CH_4 oxidation, and N_2 from NH_3 oxidation. Plume neutral gas measurements by the Cassini Ion Neutral Mass Spectrometer (INMS) instrument [*Waite et al.*, 2006] do not distinguish N_2 from CO, but if N_2 output is significant as now indicated by recent modelling of data from the Cassini Plasma Spectrometer [*Smith et al.*, 2007], active cryovolcanism and associated outgassing on Enceladus today could be a model for early formation of gravitationally bound N_2 atmospheres on more massive icy bodies such as Titan [*Owen*, 2000; *Niemann et al.*, 2005].

Laboratory data [*Loeffler et al.*, 2006b] indicate that NH_3 in thin films of water ice reacts strongly with radiolytic products of direct energetic particle irradiation to form N_2 gas, but near-infrared surface measurements [*Brown et al.*, 2006] at Enceladus find no evidence for NH_3 above trace abundances less than one percent relative to H_2O. This low surface abundance is consistent with a similar upper limit 0.5 % reported from neutral plume gas measurements by the Cassini Ion Neutral Mass Spectrometer [*Waite et al.*, 2006]. Any NH_3 brought to the surface of Enceladus by rheological transport, or as redeposited to the surface with plume ejecta, is then destroyed rapidly by direct irradiation processes. Absence of NH_3 and other reduced compounds above trace levels also means that oxidants can accumulate near the surface without immediate losses to oxidation of these compounds. This circumstance motivates our stratigraphic model (Figure 1) in which oxidant layers are transported downward from the surface to interact with layers of reduced compounds similarly transported upward from deep primordial reservoirs.

Chemical energy introduced by radiolytic oxidant production at icy surfaces provides an energy source for cryovolcanic activity and could be particularly effective in warm ice and liquid near-surface environments suggested [*Porco et al.*, 2006; *Spencer et al.*, 2006] for Enceladus. The young geologic age from crater counts in the south polar region [*Porco et al.*, 2006], and a current model for polar reorientation by diapirism [Nimmo and Pappalardo, 2006], could indicate ongoing material exchange between the irradiated surface, the subsurface source layers for the visible plumes, and the deeper interior. Despite assumptions in other Enceladus plume models to the contrary [*Matson et al.*, 2006], this vertical transport cycle apparently does not extend to the moon's ice mantle boundary with the hot rocky core, since no Europa-like [*McCord et al.*, 1998a, 1998b] mineral salt species from rocky material are detected at the surface. Lack of Europa-like non-ice material extrusion or ejection to the surface, relative to water ice deposition [*Verbiscer et al.*, 2007], is likely why Enceladus maintains its high visual albedo. Similar considerations may apply to internal transport within bright Kuiper Belt Objects, perhaps with darker objects being so due to lesser internal differentiation during primordial formation as compared to the brighter objects.

Sublimation of the H_2O ice matrix in the warm [*Spencer et al.*, 2006] (145 K) south polar region could produce high H_2O_2 concentrations [*Loeffler et al.*, 2006a] which could migrate to the subsurface environment in warm ice flows. High solubility of H_2O_2 in liquid H_2O would greatly increase downward and lateral transport rates in near-surface melt water or brine flows and within subsurface water reservoirs. Highly exothermic molecular reactions of the oxidants could occur in liquid phase with a near-surface reservoir of dissolved reductants (e.g., NH_3) in solution with H_2O, or in solid-state phase with hydrate forms of reductants as illustrated in Figure 1. Mixtures of H_2O and H_2O_2 have lower freezing temperatures than pure H_2O and may be energetically favored in early and present cryospheric environments of Earth [*Liang et al., 2006*], Mars [*Schulze-Makuch and Houtkooper*, 2006; *Houtkooper and Schulze-Makuch*, 2006], Europa [*Chyba and Hand*, 2001], and elsewhere for biological evolution.

The illustration in Figure 1 shows a variety of oxidant and reductant species, but for this report we focus on sequences starting with the catalytic dissociation of H_2O_2 to O_2 in the presence of a thermal gradient on the ice margin of a subsurface fluid reservoir and of a metal catalyst X. Exothermic reaction sequences can be ignited in H_2O-NH_3 or H_2O-CH_4 mixtures by the hot O_2 from H_2O_2 dissociation. The principal reaction equations and associated exothermic heat outputs are as follows:

$$H_2O_2 + X \rightarrow O_2 \qquad \Delta H_r = 98.2 \text{ kJ/mol } (1.02 \text{ eV}/H_2O_2)$$
$$4NH_3 + 3O_2 \rightarrow 2N_2 + 6H_2O \qquad \Delta H_r = 1359 \text{ kJ/mol } (14.1 \text{ eV}/NH_3)$$
$$CH_4 + 2O_2 \rightarrow CO_2 + 2H_2O \qquad \Delta H_r = 890 \text{ kJ/mol } (9.2 \text{ eV}/CH_4)$$

The activation energy needed to initiate these reactions can be provided in-situ by the initial H_2O_2 dissociation or by catalytic reactions of radicals such as OH or HO_2. The subsequent oxidation of NH_3 and CH_4 respectively forms N_2, CO, or CO_2 gases as drivers for cryovolcanic activity. The H_2O_2 dissociation can be catalysed even in low temperature environments by trace abundances of dissolved transition metal ions (e.g., Ti, V, Fe, Ni, Cu, Zn, Mo). Silver or platinum catalysis of H_2O_2 monopropellent at concentrations of 70 – 98 % in water is used to produce hot (>873 K) steam mixtures of the H_2O and O_2 combustion products in rocket propulsion systems [*Andrews*, 1990]. OH and HO_2 radicals are catalytically produced in the Fenton's Reagent-like transition metal decomposition of H_2O_2. Iron in the form of $FeSO_4$ salt is the typical catalyst for Fenton's Reagent reactions and the metal is universally abundant as a potential catalytic agent for Enceladus. Since we are mainly concerned with visible cryovolvanic activity in the near-surface environments of icy bodies, these low-temperature catalytic reactions may be more directly linked to such activity than high-temperature [*Matson et al.*, 2007] (500 – 800 K) reactions, e.g. for endothermic NH_3 dissociation ($2NH_3 \rightarrow N_2 + 3H_2$), in the deep interior of Enceladus and other icy moons.

Ammonia has not yet been identified at Enceladus from initial Cassini Ion Neutral Mass Spectrometer (INMS) measurements of the neutral plume gas [*Waite et al.*, 2006], but nitrogen as an atomic or molecular ion is certainly present in the magnetospheric plasma of Saturn at the orbit of Enceladus [*Smith et al.*, 2005; *Sittler et al.*, 2005; *Sittler et al.*, 2006]. Cassini Plasma Spectrometer (CAPS) measurements for radial distributions of nitrogen ions are consistent [*Smith et al.*, 2007] with a molecular nitrogen source at Enceladus. Apparent low abundance <1% of NH_3 in the neutral gas does not rule out presence of ammonia in other forms such as the ammonium ion NH_4^+, highly abundant at neutral pH in H_2O–NH_3 fluid mixtures and indistinguishable from H_2O^+ at the same mass/charge in plasma ion data. Alternatively, H_2O_2 oxidation of NH_3 may be rapid in the fluid state and consistent with absence of these species in the plume gas. As depicted in Figure 1, the primary reaction sites contributing to plume gas production might occur at lower but more sustainable rates in hydrate [*Kieffer et al.*, 2006] phases within warm ice in boundary regions surrounding a central liquid reservoir with the main non-H_2O components being gaseous products of oxidation from these regions.

The advantage of gas-driven fluid flow models for cryovolcanism is that modest molar production rates for gas can lead to much larger mass ejection rates for incompressible fluids. The measured [*Waite et al.*, 2006] volatile gas abundances relative to H_2O at Enceladus correspond to a gas-rich subsurface source environment at a total pressure ~ 10^2 bars. Bubbles of hot, 10^3 K, gas emerging at this pressure into, and rising within, a water reservoir would expand until pressure and temperature equalize with respect to the ambient hydrostatic environment. At the one-bar level, nearly equivalent to one kilometer depth in pure 273 K water at surface gravitational acceleration g ~ 0.1 m s^{-2}, the mass flow ratio of displaced water and N_2 gas is 800:1 as used for the plume flow rates in Table 1. This ratio proportionately increases for declining hydrostatic pressure toward the surface until water depths less than ten meters [*Porco et al.*, 2006] at which sublimation vapour pressure exceeds hydrostatic pressure. Thus a liquid near-surface environment has an advantage in our model of high mass ejection for plume fluid relative to gas production.

Enceladus offers the best available test for cryovolcanic models, since in-situ flyby measurements are available from the ongoing Cassini mission with more planned in the future. At minimum flow speeds of 240 m s^{-1} for gravitational escape, the measured or inferred quantities are H_2O mass loss rates: 3 – 90 kg s^{-1} from direct neutral gas measurements [*Waite et al.*, 2006], 150 – 350 kg s^{-1} from far ultraviolet absorption [*Hansen* *et al.*, 2006], and up to 100 kg s^{-1} from plasma flow deflection by pickup ion mass loading [*Tokar et al.*, 2006]. Averaged over the south polar cap region of area 72,220 km^2 southward of 55°S, these limits respectively correspond to kinetic power, delivered to the subsurface reservoir fluid in our model by oxidation product gases, of 0.001 – 0.04, 0.06 – 0.14, and 0.04 mWm^{-2}. Neutral gas data [*Waite et al.*, 2006] also suggest a narrow density spike of mass flow ~0.015 kg s^{-1} near Cassini closest approach. Overall gas data allow a large range of spatial and temporal variability in the flow.

As discussed in the next section, the energy fluxes delivered to the south polar region of Enceladus by magnetospheric electron and cosmic ray proton irradiation, and the heat fluxes arising from oxidative reactions, overlap the plume flow power requirements. However, the model gas production rates from radiolytic oxidation are near, or well below, measured lower limits on plume emissions for the product gases and suggest that relatively high abundances of gas have already accumulated in a liquid fluid reservoir after depletion of dissolved NH_3. That is, the current radiolytic oxidant input could maintain the kinetic power of the plume flows but presently be uncorrelated to the cumulative non-H_2O gas composition of the fluid. This suggests a gas-driven cryovolcanic system that is presently in high output phase but that will eventually decline in output as the reservoir gas pressure is released until more gas accumulates as we expect from oxidation of reductant fuels. Since the inflowing chemical energy from radiolysis is continuous, and the potential fuel reservoir from the moon interior is large, there could be many cycles of high and low activity in the familiar pattern of the Old Faithful geyser at Yellowstone National Park on Earth.

Another measured quantity from Cassini measurements is the ~80 mWm^{-2} average surface power of the total 5.8 GW thermal emission from the south polar cap [*Spencer et al.*, 2006] of Enceladus below 55°S. If this emission level were continuous, our estimates on steady-state radiolytic inputs, as discussed in the next section, would be far too low to account for it. However, even the globally averaged (area = 798,650 km^2) tidal and radiogenic internal heating [*Porco et al.*, 2006], each being about 0.5 GW (0.6 mWm^{-2}) and comparable to the incident energy flux (Table 1) at the global surface from magnetospheric electrons, fall far short as well. The peak temperature of the measured thermal emission at 145 K [Spencer *et al.*, 2006] is far too low [e.g., *Matson et al.*, 2007] to ignite the oxidation sequences producing CO_2 and N_2 from hydrocarbons and ammonia, so any direct link between the heat, water plume, and gas emissions remains highly speculative. Since heat may be retained for long intervals within a body of sufficiently low thermal conductivity [*Kargel*, 2006], the current thermal emission could be from an earlier transient pulse of high internal heating. Conceivably this heat pulse might have created or expanded the putative liquid reservoir. The enhanced thermal environment would not directly create cryovolcanic gases but would do so indirectly through acceleration of catalytic reactions such as we discuss for the radiolytic model.

Radiolytic oxidant accumulation in the ice crust over tens of thousands of years or longer could account for transient heat emission and plume activity even at current levels, e.g. if large clumps of peroxide-saturated ice had recently come into contact with concentrations of ammonia or other fuels as illustrated in Figure 1. The relatively distinct layers of oxidants and frost depicted in this figure would break up into clumpier concentrations during downward rheological transport and could aggregate into distributions of many smaller clumps and some large clumps over time. Lower freezing temperature of H_2O_2-enriched ice could produce more concentrated pockets of H_2O_2 over successive local melting and freezing cycles in the vicinity of the liquid reservoir. Relatively explosive activity may explain the large increase of February 2004 in neutral oxygen density observed via ultraviolet emissions [*Esposito et al.*, 2005] as Cassini approached the Saturn system. The inferred doubling of E-ring mass by 5×10^8 kg and subsequent dissipation to previous mass level over a two-month period is equivalent to Enceladus outgassing at 100 kg/s over this same period.

Energy Input and Gas Production

The Cassini Orbiter has now flown several times across the jovicentric orbit of Enceladus, but measurements of the energetic particle flux environment at the orbit of this moon are also available from the past Pioneer 11 and Voyager 2 Saturn flybys. Representative flux spectra for the magnetospheric radiation environment of Enceladus and other icy moons of Saturn have been incorporated from the Pioneer and Voyager data into the SATRAD model [*Garrett et al.*, 2005] developed by NASA's Jet Propulsion Laboratory. The electron flux spectra from SATRAD are plotted in Figure 2 for the local magnetospheric environments of Mimas, Enceladus, Tethys, Dione, and Rhea. The respective integrated energy fluxes above 10 keV for these moons are 2.5, 0.7, 0.5, 0.4, and 0.3 mW/m^2, so Enceladus's radiation environment is of intermediate intensity in the Saturn magnetosphere.

In comparison, the energy flux at Europa in the Jupiter magnetosphere is forty times higher [*Cooper et al.*, 2001] even than at Mimas, and yet there is no evidence thus far for ongoing cryovolcanism or any other surface activity there [*Phillips et al.*, 2000]. High radiation energy flux at icy moon surfaces is evidently not sufficient to produce visible plume activity. The present cryovolcanic model further requires radiolytic product access from the irradiated surface to subsurface deposits of reductant fuels such as ammonia and methane. Cassini magnetometer data on ion cyclotron waves suggest a weaker ion source at Dione by a factor of 300 as compared to Enceladus [*Leisner et al.*, 2007]. In the context of the radiolytic model this difference is either due to correspondingly lower abundance of reductants in the upper ice crust of Dione, or to absence of a liquid subsurface reservoir in the event that reductant abundances are similar to those of Enceladus.

For Enceladus the SATRAD spectrum, shown again in Figure 3, provides a useful median sample of the moon's radiation environment even over the twenty-eight years since the Pioneer 11 flyby in 1979. Figure 3 additionally shows current low and high limits for flux distributions of electrons at Enceladus. A collection of other measured MIMI spectra is also included from several other traversals of the moon's orbit around Jupiter. These assorted measurements are mostly well bounded by the upper and lower limit spectra.

Integrated input energy, H_2O_2 production, oxidative heat, and N_2 gas fluxes from these distributions are listed in Table 1 for catalyzed exothermic dissociation of H_2O_2 to O_2 and subsequent exothermic oxidation of NH_3 to H_2O and N_2 gas. For these estimates we use the maximum measured radiolytic yield, G = 0.4, a reasonable upper limit from laboratory data [*Moore and Hudson*, 2000] for an ice crust potentially saturated with CO_2 and O_2 products of radiolytic chemistry. The plume flow rates in Table 1 are computed for N_2 gas displacement of H_2O fluid at the 1-bar pressure (1-km fluid depth) level.

The lower limits on incident energy flux come from the Cassini's Enceladus I flyby, and fluxes were substantially higher a quarter century ago during the Pioneer and Voyager flybys. Subsequent Cassini data show variable fluxes up to the SATRAD level. As a primary source of neutral gas for the Saturn magnetosphere, high plume output may suppress, via energy loss through atomic ionisation, the low-energy seed population of energetic electrons in the magnetosphere. Depletion of low energy plasma electrons in the inner magnetosphere was earlier found by Voyager as a direct indicator of electron energy loss in the E-ring and associated neutral gas environment [*Sittler et al.*, 1981]. The electron fluxes in Figure 3 are measured away from the moon and are representative of globally averaged irradiation at the surface but would vary there with longitude and latitude location. Magnetospheric magnetic fields [*Dougherty et al.*, 2006] and plasma flow [*Tokar et al.*, 2006] appear significantly perturbed around Enceladus, so energy flux at the surface may concentrate at higher values, e.g. by a factor of two, in the polar regions with reduced values at the equator. Enhancement of more dense or amorphous H_2O_2 ice in the tiger stripes region [*Newman et al.*, 2006] is consistent with polar focusing of the magnetospheric particle fluxes.

Comparative incident flux distributions are also shown in Figure 3, along with corresponding energy flux values in Table 1, for electrons at Europa [*Cooper et al.*, 2001] and for cosmic ray proton irradiation of Saturn's main rings [*Johnson et al.*, 2006] and of other icy objects [*Cooper et al.*, 2003; *Cooper et al.*, 2006] in the outer heliosphere (40 AU, heliosheath) and local interstellar medium. Cosmic ray interactions with Saturn's ring material partly accounts for the observed oxygen atmosphere of these rings through total oxidant production. The dominant oxidant energy source in the rings is presently thought to be solar ultraviolet irradiation [*Johnson et al.*, 2006], and, based on earlier work for Europa [*Cooper et al.*, 2001], we estimate ~ 0.014 mWm^{-2} as the contribution of this radiation component at the south polar cap (south of 55°S) of Enceladus. Extrapolation of the cosmic ray energy flux through Saturn's planetary magnetic field to Enceladus gives an approximate surface contribution there well below the contribution limits from magnetospheric electrons but extending more deeply into the surface. Total UV and cosmic ray energy flux contributions at the Enceladus polar cap are then of order 0.02 – 0.03 mWm^{-2}, one to two orders of magnitude below the magnetospheric electron input.

The depth profiles of time scales for accumulation of radiolytic dosages computationally sufficient to convert 90% of all irradiated H_2O ice molecules to H_2O_2 at G = 0.4 are shown in Figure 4 for the electron and proton flux spectra in Figure 3. Within the visibly sensible layer, less than 1 mm in depth for inferred ice grain sizes of order 10^2 μm [*Brown et al.*, 2006], the time scales are 10^5 years for Enceladus, 10^3 years for Europa, and 10^8 – $4x10^9$ years for the outer heliosphere and beyond. Complete conversion to H_2O_2 in the visible layer can therefore occur on moon and minor planet icy bodies, photolytic destruction and other losses being ignored, over time scales from those of terrestrial ice ages and glacial flow times to the solar system age.

On Enceladus the 10^7-year turnover of the meter-thick icy regolith layer, as approximated from a Europa model [*Cooper et al.*, 2001] of impact gardening, produces a peroxide fraction to water ice of nearly 10% in this layer. Paucity of large impact craters in the south polar region [*Porco et al.*, 2006] indicates continual resurfacing to kilometers in depth. Over the solar system age, up to ~50 m of water ice at G = 0.4 is then converted to H_2O_2 on Enceladus as compared to ~5 km within Europa's surface and to 20 cm for Kuiper Belt Objects and Saturn's rings. These values suggest that the upper ice crusts of both Enceladus and Europa, and much of the sensible and deeper impact regolith layers on KBOs, could be saturated with

H_2O_2 and other oxidants. Since the condensed thickness of Pluto's ~10-microbar N_2 atmosphere [*Elliot et al.*, 2003] is equivalent in mass to ~0.1 cm of H_2O_2, the much thicker radiolytic accumulation of H_2O_2 there may have a significant chemical impact on the atmospheric evolution of Pluto. Higher surface thicknesses ~ 10 cm to 100 m for N_2 ice on Triton [*Cruikshank et al.*, 1984], the other site of directly observed cryovolcanic activity, could easily arise from radiolytic chemistry, since that moon orbits Neptune within a hot plasma magnetospheric environment. Neptunian energetic electrons and protons provide 10^9 W energy input to Triton auroral excitation [*Krimigis et al.*, 1990] as compared to our upper limit of 1.5×10^8 W from Saturnian electrons at the south polar cap of Enceladus. Greater distance from the Sun at Triton would further increase relative importance of the local radiolytic energy source as compared to previously discussed solar energy sources for the Triton N_2 geysers.

Finally, limits on N_2 gas mass flux up to 0.08 kg s^{-1} from H_2O_2 dissociation to O_2 and NH_3 oxidation are given in Table 1 for all cases. Incompressible fluid displacement factors 10^3 or greater from the N_2 mass flux at fluid depths less than 1 km, the one-bar pressure level, are then sufficient to produce observed total plume mass flows 10^1 – 10^2 kg s^{-1}. However, the Cassini INMS [*Waite et al.*, 2006] measured upper limits ~0.2 – 6 kg s^{-1} for the measured number ratio N_2:H_2O of 0.04:1.0 of Enceladus plume gas are well above even the upper limit of steady-state production from the radiolytic model.

Since the energy and heat fluxes in Table 1 are comparable to limits on the plume kinetic power, the disparity in gas fluxes suggests a lack of direct coupling between radiolytic gas injection and plume gas ejection. Together with low measured limits from INMS on abundance of NH_3 in the plume gas, this disparity may indicate that the plume gas is originating from a gas-saturated subsurface environment in which local abundances of NH_3 near the liquid reservoir have recently been depleted by cumulative oxidation. Apparent lack of H_2O_2 in the plume gas, if we assume for the moment that INMS has any significant sensitivity to such reactive species, similarly argues that H_2O_2 and NH_3 react mainly in the boundary regions surrounding the putative liquid reservoir and that only the gaseous oxidation products persist in that reservoir. Future improvements in laboratory calibration of INMS with respect to reactive oxidants may change this assessment. Unless the plumes are unique to the present epoch, the depleted NH_3, also including that part lost at the surface by direct irradiation [*Loeffler et al.*, 2006b], must eventually be resupplied by upward transport of NH_3 - rich ice from the deep interior.

Discussion

The radiolytic model depends on the near-surface production of oxidants that should be present near the surface of icy bodies of the outer solar system, wherever water ice is irradiated by energetic particles and ultraviolet photons from the magnetospheric, heliospheric, or interstellar space environments of these bodies. Chemical energy accumulates in these oxidants over a vast range of time scales in different magnetospheric, and heliospheric, locations. This energy can be released when the oxidants come into contact with reductant fuels such as NH_3 and CH_4 in the presence either of high temperatures or catalytic materials Hydrogen peroxide is produced by ice radiolysis and photolysis in low-temperature environments and has the advantage of exothermic, potentially explosive, dissociation to O_2 in the presence of iron and other commonly abundant metal catalysts. No laboratory measurements are yet available on metal-catalyzed dissociation rates at the observed temperatures of 80 – 145 K on Enceladus but these rates would rapidly increase in the warmer ice surrounding a liquid water reservoir. This initial exothermic reaction could then initiate oxidation of reductants to produce volatile gases driving cryovolcanic activity. Trace hydrocarbon species, such as the INMS-detected [*Waite et al.*, 2006] acetylene and propane at Enceladus, could be produced in the high temperature sequences initiated by H_2O_2 dissociation. These species may take part in further reactions, potentially with explosive results, as found by Benit and Roessler [1993] for proton-irradiated acetylene frost at 77 K, even at the low end of the Enceladus temperature range.

Visible manifestations of cryovolcanism include emissions of ice grains, neutral gas, pickup ions, and dust, but the generally bright reflective surfaces of other icy bodies, as in the Kuiper Belt, are also highly suggestive of sustained cryovolcanism. New observations of ammonia hydrate on the surface of Charon in the Pluto system [*Cook et al.*, 2007] suggest that cryovolcanism is active there. In the Saturn magnetospheric environment the Enceladus ice grain output sustains the E-ring population which then globally bombards and brightens [*Verbiscer et al.*, 2007] the surfaces of Enceladus and other moons. Cyclic activity at Enceladus could produce stratigraphic layers (Figure 1) of high oxidant accumulation during low activity intervals and of high albedo water frost from direct plume output and surface bombardment by E-ring grains during high activity phases. Currently high plume and thermal emission suggests that Enceladus is now in its most active phase, and that any non-ice materials, including abundant oxidants expected from continuous magnetospheric irradiation, are now mostly buried from view by water ice frost from plume ejecta.

Enceladus outgassing into Saturn's magnetosphere, and resultant electron energy loss in E-ring dust and neutral gas, should lead to anti-correlation of plume output with the fluxes of energetic and lower-energy suprathermal electrons near and beyond the orbit of Enceladus. The large decrease in low energy (< 0.5 MeV) electron and energetic (> 0.5 MeV) ion fluxes inward from the orbit of Rhea (8.75 R_S) to that of Enceladus (3.75 R_S) was first discovered by Pioneer 11 measurements [*McDonald et al.*, 1980; *Simpson et al.*, 1980; *Trainer et al.*, 1980; *Van Allen et al.*, 1980]. The subsequent Voyager measurements found dropouts in suprathermal (0.03 – 6 keV) electron [*Sittler et al.*, 1981], ring current ion [*Connerney et al.*, 1981; *Acuña et al.*, 1981], and energetic (> 500 keV) ion [*Krimigis et al.*, 1981, 1983; and as reinterpreted by *Paranicas et al.*, 2004] fluxes.

These inward flux decreases are now clearly attributable to Enceladus neutral gas and E-ring ice grain interactions a quarter century after the first suggestion of a potential E-ring interaction by Thomsen and Van Allen [1979] in a report published just after the Pioneer 11 flyby. In comparison, the Pioneer and Voyager energetic electron fluxes increased with no evident E-ring interaction toward Saturn, until cutoff by the main rings, from source regions in the Enceladus – Rhea region and beyond. Generally reduced fluxes of energetic electrons near the orbit of Enceladus, as recently measured by the Cassini MIMI instrument (Figure 3), suggest that the currently high plume output may be attenuating the supply of low-energy electrons feeding via magnetospheric acceleration processes into the energetic electron population. If so, the current rate of surface oxidant production is now low but will again increase if plume output subsides and the low-energy electron source of the energetic electrons at Enceladus is no longer attenuated in diffusing inward through the E-ring region.

Negative feedback of Enceladus plume activity to the electron source could produce cyclic high phases of "Old Faithful" activity initiated after long periods of high oxidant accumulation rates during low activity phases. Cyclic plume activity elsewhere may be confined to planetary magnetospheric environments in which the cryovolcanic emissions are large enough to attenuate source fluxes of energetic particles producing the surface oxidants. In heliospheric environments the activity may be more episodic and driven by subsurface circulation of reductant fuels to the oxidant-saturated near-surface water ice environment. In all cases, interactions of clumps of highly concentrated oxidants and reductants, as in Figure 1 for Enceladus, could produce transiently high plume activity and heat output after slow accumulations over much longer time intervals, e.g. thousands of years for Enceladus as compared to the quarter-century of our present Voyager-Cassini measurements for the E-ring and now for Enceladus. In comparison, long term storage of heat, e.g. due to low thermal conductivity in the ice mantle [*Kargel*, 2006], can be theorized for alternative theories invoking episodic tidal heating, but we have yet no independent evidence for such episodes in the surface features and chemical composition of Enceladus.

Enceladus has the highest density, 1.6 g/cc, of all major Saturn satellites excluding Titan, but the sensible surface does not show composition consistent with continuing chemical contact to the requisite rocky core [*Porco et al.*, 2006] underlying the outer ice mantle at this density. There is no evidence from near-infrared imaging spectroscopy [*Brown et al.*, 2006] for surface presence of Europa-like [*McCord et al.*, 1998a, 1998b] sulfate hydrates or other non-ice species that might directly convect through warm ice crust layers to the surface or become manifested through the plume outflow. We suggest that this poses a significant problem for the widely publicized theory of *Matson et al.* [2007] that the plumes are a manifestation of high temperature (> 500 K) ammonia chemistry and resultant gas production deep in the moon interior at the core-mantle boundary. A deep source is also difficult to connect to plume variability strongly suggested by the large transient increase [*Esposito et al.*, 2005] in magnetospheric neutral gas during Feb. 2004. Such transients are more likely to arise from plume source dynamics closer to the surface.

We acknowledge the suggestions of *Kargel* [2006] and *Kieffer et al.* [2006] that gas clathrate decomposition in the presence of thermal gradients could contribute to Enceladus cryovolcanism, but production of the enclathrated gases then remains to be explained. If formed during original accretion and differentiation of Enceladus, these gases would have long since escaped, since this moon is too small to retain an atmosphere like that of Titan [*Owen*, 2000]. Sequestration of the ammonia in rocky ammonium minerals was suggested as one alternative [*Kargel*, 2006], but lack of surface compositional expression for continuous ice mantle circulation from the rock core boundary provides no current support for this alternative. The radiolytic model instead postulates that primordial ammonia, methane, and other hydrocarbon sources of cryovolcanic gases are abundant within the ice mantle, e.g. in the form of hydrates, and that gas production occurs in the warm ice basal margins of a near-surface liquid reservoir on contact with oxidants from the irradiated surface.

Even at the relatively high temperature of pure liquid water, the spontaneous dissociation of H_2O_2 to O_2 must be catalysed in the radiolytic model by non-ice contaminants, e.g. universally abundant Fe, originating either from the rocky mineral composition of the deep interior or from meteoritic bombardment. The absences of detectable minerals on the surface and of O_2 in the atmospheric environment argue that this dissociation cannot occur very near the surface, and that radiolytic H_2O_2 can continuously accumulate and concentrate in the near-surface ice environment. If the near-surface environment undergoes cyclic melting and freezing phases, the non-ice materials will accumulate as brines at lower depths below the melt layers. These contaminants will similarly have low abundances within a liquid subsurface reservoir and likely contribute only at trace levels to composition of cryovolcanic plumes. For the present model we assume that sufficient trace abundances of Fe and other metals are mixed with continuously upwelling fuels, e.g. hydrates of NH_3 and CH_4, to trigger H_2O_2 dissociation at the basal thermal margins of the fluid reservoir as depicted in Figure 1, and that these metals do not limit the accumulation of H_2O_2 above the reservoir. This vertical gradient in catalyst density allows the requisite inverse gradient in oxidant accumulation to occur and sets the stage for the exothermic reactions leading to gas production and fluid ejection to form cryovolcanic plumes. Initial vertical segregation of oxidants and fuels may be essential to the explosive form of cryvolcanism potentially accounting for the spectacular plumes of Enceladus.

Saturn kilometric radiation (SKR) provides a new diagnostic for limits on magnetospheric mass loading by ions originating from Enceladus plume gas and ice grains. During the 1980 – 1981 flybys the two Voyager spacecraft discovered these radio emissions with a periodicity of 10 hours 39 min 24 ± 7 s, then thought to arise from intrinsic rotation of Saturn [*Desch and Kaiser*, 1981]. Later Ulysses radio observations from 1994 to 1997 showed changes in SKR periodicity up to 1% relative to the Voyager observations. Initial Cassini measurements determined a more precise value of 10 hours 45 min 45±36 s [*Gurnett et al.*, 2005] for an increase of 6.35 minutes (1%) since 1980 - 1981. Slippage of the coupled magnetosphere-ionosphere system with respect to planetary rotation, due to magnetospheric plasma loading by Enceladus outgassing and subsequent ionisation of plume neutrals, is proposed [*Gurnett et al.*, 2007] to account for the radio SKR period. A theory of rotationally-driven plasma convection [*Goldreich and Farmer*, 2006] estimates the mass loading for the 1% SKR period variation at 10 kg/s radial mass outflow from Enceladus and the E-ring. Although zonal variations of Saturn's atmospheric rotation speeds presently preclude independent measurement of intrinsic planetary rotation, differential changes in SKR period could be monitored as a linear measure of Enceladus plume output. Stability of this period within 1% does imply relative stability over the last quarter century but does not limit longer term stability. Continued monitoring of SKR periodicity, as compared to Enceladus plume activity and magnetospheric particle fluxes, is needed to further quantify Enceladus two-way coupling to the magnetosphere.

The current plume flow limits of 3 - 350 kg/s for Enceladus project over the solar system age to the cumulative loss of 0.4 – 46 % from the moon's total mass. For spherical symmetry a flow rate of 70 kg/s extrapolates to complete loss of the nine percent of total moon mass southward of 55°S. Enormous redistribution of mass would have globally occurred within the deep interior if the plumes had been continuously active at such rates. A far lower limit on cumulative mass loss of 0.03%, corresponding to 0.2 kg/s in flow rate, comes from the observed ~ 0.5-km depression of the south polar cap region [*Porco et al.*, 2006], although much of the plume mass has likely returned to the surface. Thus the average flow rate may have been even much lower even than 3 kg/s, and there could have been long intervals for accumulation of stored radiolytic energy to fully account for all aspects of current plume flow and polar cap heat emission. The present epoch of high activity, manifested in the E-ring during the Voyager era of 1980 – 1981, and now seen directly by Cassini, may be a short-lived and periodic event over the history of Enceladus. An apt analogy may be Old Faithful with variable output eruptions over a few minutes at intervals of about ninety minutes. It is therefore now advisable to calibrate remote long-term indicators of plume activity, potentially including SKR emission that be monitored from Earth, to the ongoing Cassini measurements within the Saturn system.

Oxidant chemistry induced by cosmic ray irradiation could drive resurfacing on the large bright Kuiper Belt Objects such as Eris and more generally account for the diversity of surface brightness and color [*Jewitt and Luu*, 2001; *Doressoundiram et al.*, 2002] among the icy dwarf planets of the outer solar system. Water ice mantles should be common on KBOs and deep water-ice absorptions are directly seen on some objects such as the 2003 EL_{61} collisional family [*Brown et al.*, 2007; *Barkume et al.*, 2006] and Charon [*Brown and Calvin*, 2000]. Although N_2 and CH_4 ices are dominant on larger bodies such as Pluto [*Brown and Calvin*, 2000] and Eris [*Brown et al.*, 2005], surface layers of these volatile molecules would not be retained on smaller objects [*Brown and Calvin*, 2000] and, if present, would have to be renewed by outgassing from the subsurface, e.g. by cryovolvanism. Oxidant production from cosmic ray irradiation of visible surface or near-surface water ice must therefore be accounted for as one chemical energy source for potential cryovolcanic activity of these objects. The respective Voyager 2 and Cassini flyby observations have given the first close looks at active cryovolcanism on Triton and Enceladus. New Horizons is our next opportunity to search for such activity at Pluto and Charon during the April 12, 2015 flyby of this icy dwarf planet system.

Finally, the suggested vertical segregation of near-surface radiolytic oxidants and deeper-lying reductant fuels on irradiated icy bodies potentially provides chemical energy resources for future exploration and habitation of the outer solar system and beyond. Since heliocentric orbits of many of these bodies, such as Centaurs, are dynamically unstable, oxidant and fuel mining can be envisaged on icy objects having more recently entered the inner solar system after billions of years of radiolytic processing in the Kuiper Belt or Oort Cloud regions. If there is ever the need to divert such an object from impact with the Earth, this potentially accessible chemical redox energy accumulated within the body could become a critical resource. In these respects, if the radiolytic model proves to be correct, Enceladus may be viewed not only as an object of intense scientific interest but also as a natural model for astroengineering. Sagan [1994] suggested utilization of icy bodies as spaceships to other stars, and Enceladus may be a spectacularly visible model for fulfilment of this vision.

References

Acuña, M. H., J. E. P. Connerney, and N. F. Ness (1981), Topology of Saturn's main magnetic field, *Nature*, *292*, 721-724.

Andrews, D. (1990), Advantages of hydrogen peroxide as a rocket oxidant, *J. Brit. Interplan. Soc.*, *43*, 319-328.

Barkume, K. M., M. E. Brown, and E. L. Schaller (2006), Water ice on the satellite of Kuiper belt object 2003 EL_{61}, *Astrophys. J.*, *640*, L87-L89.

Benit, J., and K. Roessler (1993), Explosive processes in frozen acetylene irradiated by MeV protons (cosmic ray simulation), in *Astronomical Infrared Spectroscopy: Future observational directions*, edited by S. Kwok, *ASP Conf. Ser. 41*, pp. 277-278, Astron. Soc. Pacific.

Brown, M. E, and W. M. Calvin (2000), Evidence for crystalline water and ammonia ices on Pluto's satellite Charon, *Science*, *287*, 107-109.

Brown, M. E., C. A. Trujillo, and D. L. Rabinowitz (2005), Discovery of a planetary-sized object in the Scattered Kuiper Belt, *Astrophys. J. Lett.*, *635*, L97-L100.

Brown, R. H., R. L. Kirk, T. V. Johnson, and L. A. Soderblom (1990), Energy sources for Triton's geyser-like plumes, *Science*, *250*, 431-435.

Brown, R. H., et al. (2006), Composition and physical properties of Enceladus' surface, *Science*, *311*, 1425-1428.

Brown, M. E., K. M. Barkume, D. Ragozzine, and E. L. Schaller (2007), A collisional family of icy objects in the Kuiper Belt, *Nature*, *446*, 294-296.

Buratti, B. J., et al. (2005), Cassini Visual and Infrared Mapping Spectrometer observations of Iapetus: Detection of CO_2, *Astrophys. J.*, *622*, L149-L152.

Carlson, R. W. (1999), A tenuous carbon dioxide atmosphere on Jupiter's moon Callisto, *Science*, *283*, 820-821.

Carlson, R., et al. (1999), Hydrogen peroxide on the surface of Europa, *Science*, *283*, 2062-2064.

Chyba, C. F., and K. P. Hand (2001), Life without photosynthesis, *Science*, *292*, 2026-2027.

Connerney, J. E. P., M. H. Acuña, and N. F. Ness (1981), Saturn's ring current and inner magnetosphere, *Nature*, *292*, 724-726.

Cook, J. C., S. J. Desch, T. L. Roush, C. A. Trujillo, and T. R. Geballe (2007), Near-infrared spectroscopy of Charon: Possible evidence for cryovolcanism on Kuiper Belt Objects, *Astrophys. J.*, *663*, 1406–1419.

Cooper, J. F., R. E. Johnson, B. H. Mauk, H. B. Garrett, and N. Gehrels (2001), Energetic ion and electron irradiation of the icy Galilean satellites, *Icarus*, *149*, 133-159.

Cooper, J. F., E. R. Christian, J. D. Richardson, and C. Wang (2003), Proton irradiation of Centaur, Kuiper Belt, and Oort Cloud objects at plasma to cosmic ray energy, *Earth Moon Plan.*, *92*, 261-277.

Cooper, J. F., M. E. Hill, J. D. Richardson, and S. J. Sturner (2006), Proton irradiation environment of solar system objects in the heliospheric boundary regions, in *Physics of the Inner Heliosheath, Voyager Observations, Theory, and Future Prospects; 5th Annual IGPP International Astrophysics Conference*, edited by J. Heerikhuisen, V. Florinski, G.P. Zank and N.V. Pogorelov, *AIP Conf. Proc. 858*, pp. 372-379.

Cruikshank, D. P., R. H. Brown, and R. G. Clark (1984), Nitrogen on Triton, *Icarus*, *58*, 293-305.

Cruikshank, D. P., T. L. Roush, J. M. Moore, M. Sykes, T. C. Owen, M. J. Bartholomew, R. H. Brown, and K. A. Tryka (1997), The surfaces of Pluto and Charon, in *Pluto and Charon*, edited by S. A. Stern, and D. J. Tholen, p. 211, University of Arizona Press, Tucson.

Divine, N., and H. B. Garrett (1983), Charged particle distributions in Jupiter's magnetosphere, *J. Geophys. Res.*, *88*, 6889–6903.

Doressoundiram, A., N. Peixinho, C. de Bergh, S. Fornasier, Ph. Thébault, M. A. Barucci, and C. Veillet (2002), The color distribution in the Edgeworth-Kuiper Belt, *Astron. J.*, *124*, 2279-2296.

Dougherty, M. K., K. K. Khurana, F. M. Neubauer, C. T. Russell, J. Saur, J. S. Leisner, and M. E. Burton (2006), Identification of a dynamic atmosphere at Enceladus with the Cassini Magnetometer, *Science*, *311*, 1406-1409.

Esposito, L., et al. (2005), Ultraviolet imaging spectroscopy shows an active Saturnian system, *Science*, *307*, 1251-1255.

Formisano, V., S. Atreya, T. Encrenaz, N. Ignatiev, and M. Giuranna (2004), Detection of methane in the atmosphere of Mars, *Science*, 306, 1758-1761.

Garrett, H. B., J. M. Ratliff, and R. W. Evans (2005), Saturn Radiation (SATRAD) Model, JPL Pub. 05-09, NASA Jet Propulsion Lab.

Goldreich, P., and A. J. Farmer (2006), Spontaneous axisymmetry breaking of Saturn's external magnetic field, *J. Geophys. Res.*, *112*, A05225, doi:10.1029/2006JA012163.

Gomis, O., G. Leto, and G. Strazzulla (2004a), Hydrogen peroxide production by ion irradiation of thin water ice films, *Astron. Astrophys.*, *420*, 405-410.

Gomis, O., M. A. Satorre, G. Strazzulla, and G. Leto (2004b), Hydrogen peroxide formation by ion implantation in water ice and its relevance to the Galilean satellites, *Plan. Sp. Sci.*, *52*, 371-378.

Gurnett, D. A., A. M. Persoon, W. S. Kurth, J. B. Groene, T. F. Averkamp, M. K. Dougherty, and D. J. Southwood (2007), The variable rotation period of the inner region of Saturn's plasma disk, *Science*, *316*, 442-445.

Hall, D. T., D. F. Strobel, P. D. Feldman, M. A. McGrath, and H. A. Weaver (1995), Detection of an oxygen atmosphere on Jupiter's moon Europa, *Nature*, *373*, 677-679.

Hall, D. T., P. D. Feldman, M. A. McGrath, and D. F. Strobel (1998), The far-ultraviolet oxygen airglow of Europa and Ganymede, *Astrophys. J.*, *499*, 475-481.

Hansen, C. J., L. Esposito, A. I. F. Stewart, J. Colwell, A. Hendrix, W. Pryor, D. Shemansky, and R. West (2006), Enceladus' water vapor plume, *Science*, *311*, 1422-1425.

Hendrix, A. R., C. A. Barth, and C. W. Hord (1999a), Ganymede's ozone-like absorber: Observations by the Galileo ultraviolet spectrometer, *J. Geophys. Res.*, *104*, 14169-14178.

Hendrix, A. R., C. A. Barth, A. I. F. Stewart, C. W. Hord, and A. L. Lane (1999b), Hydrogen peroxide on the icy Galilean satellites, paper presented at 30th Annual Lunar and Planetary Science Conference, March 15-29, 1999, Houston, TX, Abstract No. 2043.

Hibbitts, C. A., T. B. McCord, and G. B. Hansen (2000), Distributions of CO_2 and SO_2 on the surface of Callisto, *J. Geophys. Res.*, *105*, 22541-22557.

Hibbitts, C. A., J. E. Klemaszewski, T. B. McCord, G. B. Hansen, and R. Greeley (2002), CO_2-rich impact craters on Callisto, *J. Geophys. Res.*, *107*, 5084, doi:10.1029/2000JE001412.

Hibbitts, C. A., R. T. Pappalardo, G. B. Hansen, and T. B. McCord (2003), Carbon dioxide on Ganymede, *J. Geophys. Res.*, *108*, 5036, doi:10.1029/2002JE001956.

Houtkooper, J. M., and D. Schulze-Makuch (2007), A possible biogenic origin for hydrogen peroxide on Mars: the Viking results reinterpreted, *Int. J. Astrob.*, *6*, 147-152.

Jewitt, D. C., and J. X. Luu (2001), Colors and spectra of Kuiper Belt objects, *Astron. J.*, *122*, 2099-2114.

Johnson, R. E., R. W. Carlson, J. F. Cooper, C. Paranicas, M. H. Moore, and M. C. Wong (2004), Radiation effects on the surfaces of the Galilean satellites, In *Jupiter - The Planet,* *Satellites and Magnetosphere*, edited by F. Bagenal, W. B. McKinnon, and T. E. Dowling, pp. 485-512, Cambridge Univ. Press, New York.

Johnson, R. E., J. G. Luhmann, R. L. Tokar, M. Bouhram, J. J. Berthelier, E. C. Sittler, J. F. Cooper, T. W. Hill, H. T. Smith, M. Michael, M. Liu, F. J. Crary, and D. T. Young (2006), Production, ionization and redistribution of O_2 in Saturn's ring atmosphere, *Icarus*, *180*, 393-402.

Kargel, J. S. (2006), Enceladus: Cosmic gymnast, volatile miniworld, *Science*, *311*, 1389-1391.

Kieffer, S. W., X. Lu, C. M. Bethke, J. M. Spencer, S. Marshak, and A. A. Navrotsky (2006), Clathrate reservoir hypothesis for Enceladus' south polar plume, *Science*, *314*, 1764-1766.

Kirk, R. L., R. H. Brown, and L. A. Soderblom (1990), Subsurface energy storage and transport for solar-powered geysers on Triton, *Science*, *250*, 424-429.

Kivelson, M. G., F. Bagenal, W. S. Kurth, F. M. Neubauer, C. Paranicas, and J. Saur (2004), Magnetospheric interactions with satellites, In *Jupiter - The Planet, Satellites and Magnetosphere*, edited by F. Bagenal, W. B. McKinnon, and T. E. Dowling, pp. 513-536, Cambridge Univ. Press, New York.

Krimigis, S. M., et al. (1989), Hot plasma and energetic particles in Neptune's magnetosphere, *Science*, *246*, 1483-1489.

Krimigis, S. M., et al. (2004), Magnetosphere Imaging Instrument (MIMI) on the Cassini Mission to Saturn/Titan, *Sp. Sci. Rev.*, *114*, 233-329.

Leisner, J. S., K. K. Khurana, C. T. Russell, M. K. Dougherty, A. M. Persoon, X. Blanco-Cano, and R. J. Strangeway (2007), Observations of Enceladus and Dione as sources for Saturn's neutral cloud, paper presented at 38th Annual Lunar and Planetary Science Conference, Houston, TX, Abstract No. 1425.

Liang, M.C., B. F. Lane, R. T. Pappalardo, M. Allen, and Y. L. Yung (2005), Atmosphere of Callisto, *J. Geophys. Res.*, *110*, E02003, 10.1029/2004JE002322.

Liang, M.-C., H. Hartman, R. E. Kopp, J. L. Kirschvink, and Y. L. Yung (2006), Production of hydrogen peroxide in the atmosphere of a Snowball Earth and the origin of oxygenic photosynthesis, *PNAS, 103*, 18896-18899.

Loeffler, M. J., U. Raut, R. A. Vidal, R. A. Baragiola, and R. W. Carlson (2006a), Synthesis of hydrogen peroxide in water ice by ion irradiation, *Icarus*, *180*, 265-273.

Loeffler, M. J., U. Raut, and R. A. Baragiola (2006b), Enceladus: A source of nitrogen and an explanation for the water, *Astrophys. J.*, *649*, L133-L136.

Matson, D. L., J. C. Castillo, J. Lunine, and T. V. Johnson (2007), Enceladus' plume: Compositional evidence for a hot interior, *Icarus*, *187*, 569-573.

Maurice, S., E. C. Sittler, J. F. Cooper, B. H. Mauk, M. Blanc, and R. S. Selenick (1996), Comprehensive analysis of electron observations at Saturn: Voyager 1 and 2, *J. Geophys. Res.*, *101*, 15211-15232.

McCord, T. B., et al. (1998a), Salts on Europa's surface detected by Galileo's Near Infrared Mapping Spectrometer, *Science*, *280*, 1242-1245.

McCord, T. B., et al. (1998b), Non-water-ice constituents in the surface material of the icy Galilean satellites from the Galileo near-infrared mapping spectrometer investigation, *J. Geophys. Res.*, *103*, 8603-8626.

McKinnon, W. B. (2006), On convection in ice I shells of outer Solar System bodies, with detailed application to Callisto, *Icarus*, *183*, 435-450.

McKinnon, W. B., and A. C. Barr (2006), Structure and evolution of ice dwarf planets, *Bull. Amer. Astron. Soc.*, *38*, 518.

Moore, M. H., and R. L. Hudson (2000), IR detection of H_2O_2 at 80 K in ion-irradiated laboratory ices relevant to Europa, *Icarus*, *145,* 282-288.

Mumma, M. J., R. E. Novak, M. A. DiSanti, B. P. Bonev, and N. Dello Russo (2004), Detection and mapping of methane and water on Mars, *Bull. Amer. Astron. Soc.*, *36*, 1127.

Newman, S. F., B. J. Buratti, R. H. Brown, R. Jaumann, J. Bauer, and T. Momary (2007), The search for hydrogen peroxide on Enceladus, Lunar and Planetary Institute Conference Abstracts, *38*, 1769.

Niemann, H. B., et al. (2005), The abundances of constituents of Titan's atmosphere from the GCMS instrument on the Huygens probe, *Nature*, *438*, 779-784.

Nimmo, F., and R. T. Pappalardo (2006), Diapir-induced reorientation of Saturn's moon Enceladus, *Nature, 441*, 614-616.

Noll, K. S., R. E. Johnson, A. L. Lane, D. L. Domingue, and H. L. Weaver (1996), Detection of ozone on Ganymede, *Science*, *273*, 341-343.

Noll, K. S., T. L. Roush, D. P. Cruikshank, R. E. Johnson, and Y. J. Pendleton (1997), Detection of ozone on Saturn's satellites Rhea and Dione, *Nature*, *388*, 45-47.

Owen, T. C. (2000), On the origin of Titan's atmosphere, *Plan. Sp. Sci., 48*, 747-752.

Pappalardo, R. T., et al. (1999), Does Europa have a subsurface ocean? Evaluation of the geological evidence, *J. Geophys. Res.*, *104*, 24015-24055.

Paranicas, C., R. B. Decker, B. H. Mauk, S. M. Krimigis, T. P. Armstrong, and S. Jurac (2004), Energetic ion composotion in Saturn's magnetosphere revisited, *Geophys. Res. Lett.*, *31*, L04810, doi:10.1029/2003GL018899.

Phillips, C. B., A. S. McEwen, G. V. Hoppa, S. A. Fagents, R. Greeley, J. E. Klemaszewski, R. T. Pappalardo, K. P. Klaasen, and H. H. Breneman (2000), The search for current geologic activity on Europa, *J. Geophys. Res.*, *105*, 22579-22597.

Porco, C. C., et al. (2006), Cassini observes the active south pole of Enceladus, *Science*, *311*, 1393-1401.

Sagan, C. (1994), *Pale Blue Dot: A Vision of the Human Future in Space*, 1st edition, ISBN 0-679-43841-6, Random House, New York.

Schulze-Makuch, D., and J. M. Houtkooper (2006), Life on Mars? Reinterpretation of the Viking life detection experiments: A possible biogenic origin of hydrogen peroxide, *Amer. Astron. Soc. Meeting Abstracts*, *209*, 35.03.

Sittler, E. C., J. D. Scudder, and H. S. Bridge (1981), Distribution of neutral gas and dust near Saturn, *Nature*, *292*, 711-714.

Sittler, E. C., Jr., et al. (2005), Preliminary results on Saturn's inner plasmasphere as observed by Cassini: Comparison with Voyager, *Geophys. Res. Lett.*, *32*, L14S07, doi:10.1029/2005GL022653.

Sittler, E. C., Jr., et al. (2006), Energetic nitrogen atoms within the inner magnetosphere of Saturn, *J. Geophys. Res.*, *111*, A09223, doi:10.1029/2004JA010509.

Smith, H. T., M. Shappirio, E. C. Sittler, D. Reisenfeld, R. E. Johnson, R. A. Baragiola, F. J. Crary, D. J. McComas, and D. T. Young (2005), Discovery of nitrogen in Saturn's inner magnetosphere, *Geophys. Res. Lett.*, *32*, L14S03, 10.1029/2005GL022654.

Smith, H. T., R. E. Johnson, E. C. Sittler, M. Shappirio, D. Reisenfeld, O. J. Tucker, M. Burger, F. J. Crary, D. J. McComas, and D. T. Young (2007), Enceladus: The likely dominant nitrogen source in Saturn's magnetosphere, *Icarus*, *88*, 356-366.

Soderblom, L. A., T. L. Becker, S. W. Kieffer, R. H. Brown, C. J. Hansen, and T. V. Johnson (1990), Triton's geyser-like plumes: Discovery and basic characterization, *Science*, *250*, 410-415.

Spahn, F., et al. (2006), Cassini dust measurements at Enceladus and implications for the origin of the E ring, *Science*, *311*, 1416-1418.

Spencer, J. R., W. M. Calvin, and M. J. Person (1995), Charged-coupled device spectra of the Galilean satellites: molecular oxygen on Ganymede, *J. Geophys. Res.*, *100*, 19049-19056.

Spencer, J. R., and W. M. Calvin (2002), Condensed O_2 on Europa and Callisto, *Astron. J.*, *124*, 3400-3403.

Strobel, D. F., J. Saur, P. D. Feldman, and M. A. McGrath, Hubble Space Telescope Space Telescope Imaging Spectrograph search for an atmosphere on Callisto: A jovian unipolar inductor (2002), *Astrophys. J.*, *581*, L51-L54.

Spencer, J. R., J. C. Pearl, M. Segura, F. M. Flasar, A. Mamoutkine, P. Romani, B. J. Buratti, A. R. Hendrix, L. J. Spilker, and R. M. C. Lopes (2006), Cassini encounters Enceladus: Background and the discovery of a south polar hot spot, *Science, 311*, 1401–1405.

Sturner, S. J., et al. (2003), Monte Carlo simulations and generation of the SPI response, *Astron. Astrophys.*, *411*, L81-L84.

Tokar, R. L., et al. (2006). The interaction of the atmosphere of Enceladus with Saturn's plasma, *Science*, *311*, 1409-1412.

Verbiscer, A., R. French, M. Showalter, and P. Helfenstein (2007), Enceladus: Cosmic graffiti artist caught in the act, *Science*, *315*, 815.

Waite, J. H., et al. (2006), Cassini Ion and Neutral Mass Spectrometer: Enceladus plume composition and structure, *Science*, *311*, 1419-1422.

Williams, D. J., R. W. McEntire, S. Jaskulek, and B. Wilken (1992), The Galileo Energetic Particles Detector, *Sp. Sci. Rev.*, *60*, 385–412.

Ziegler, J. F., J. P. Biersack, and U. Littmark (1985), *The Stopping and Range of Ions in Solids*, Pergamon Press, New York.

Acknowledgements. This work was supported in part by the Cassini Plasma Spectrometer (CAPS) Project and the Space Physics Data Facility at Goddard Space Flight Center.

Table 1. Radiolytic Cryovolcanism Model Parameters for Enceladus

Body – Model	Particle Energy Flux mWm^{-2}	H_2O_2 Number Flux* $(cm^2\text{-}s)^{-1}$	Chemical Heat Flux mWm^{-2}	N_2 Source Flow $kg\ s^{-1}$	Plume Fluid Flow $kg\ s^{-1}$
Europa – e	100	$1.7x10^{11}$	5.4	3.8	3000
Enc – high e	2.1	$3.6x10^{9}$	0.11	0.08	64
Enc – mid e	0.7	$1.2x10^{9}$	0.039	0.027	22
Enc – low e	0.1	$1.7x10^{8}$	0.0054	0.0038	3.0
Enc – CRP	0.002	$3.4x10^{6}$	0.00011	$7.7x10^{-5}$	0.062
Rings – CRP	0.0005	$8.5x10^{5}$	$2.7x10^{-5}$	$1.9x10^{-5}$	0.015
40AU SolMin - CRP	0.003	$5.2x10^{6}$	0.00016	0.00012	0.096
HS – CRP	0.0035	$6.0x10^{6}$	0.00019	0.00013	0.10
LISM – CRP	0.0083	$1.4x10^{7}$	0.00044	0.00032	0.26

*Computed at maximum radiolytic yield G = 0.4 for H_2O_2.

Abbeviations: Enc – X – e (high, middle, and low electron flux models for Enceladus), CRP (cosmic ray proton), Ring (Saturn's main rings), SolMin (solar minimum), HS (heliosheath), LISM (local interstellar medium).

Figure Captions

Figure 1. Illustration of radiolytic gas-driven cryovolvanism for potential subsurface liquid water reservoir near the surface of Enceladus. A continuous rain of energetic electrons (yellow arrows) drives radiolysis and saturates the upper ice surface with oxidants (blue), mostly H_2O_2 but with mix of other species. Transient plume activity ejects ice grains falling back to the surface (white ballistic curves) and depositing multiple layers of water frost (white) interspersed with oxidant concentrations accumulating during lower plume activity. Ice upwelling continuously supplies fresh "fuels" (red), e.g. hydrates of CH_4 and NH_4, from the deep interior. Exposure to increasing temperature within the ice margins of the fluid reservoir initiates sequences of exothermic reactions from H_2O_2 dissociation to fuel oxidation, resultant gas production, and fluid reservoir heating. Percolation of expanding hot gas bubbles from the margins into the incompressible water fluid becomes the driving force for upward movement (white arrows) of gas-saturated fluid to form the plumes. Interactions of lower (left side) or higher (right side) concentrations of oxidants and fuels produce correspondingly less or more gas.

Figure 2. Representative differential flux spectra of Saturn magnetospheric electrons at the equatorial jovicentric orbits of the icy moons Mimas, Enceladus, Tethys, Dione, and Rhea as determined from the SATRAD model [*Garrett et al.*, 2005].

Figure 3. Differential flux spectra of energetic electrons (red curves) at Enceladus and Europa, respectively from the planetary magnetospheres of Saturn and Jupiter, and of cosmic ray protons (black curves) irradiating icy bodies within and beyond the heliosphere. The thickest solid Enceladus curve is from the SATRAD model. The two medium-thickness Enceladus curves are respectively upper and lower limits from Voyager and Cassini/MIMI electron data. The upper limit comes from Voyager measurements compiled by *Maurice et al.* [1996], and the lower limit is from Cassini electron flux measurements by the Magnetospheric Imaging Instrument (MIMI) experiment [*Krimigis et al.*, 2004] near the

Jupiter-fixed longitude of this moon during the 9 March 2005 flyby. The limiting flux curves for Enceladus are extrapolated into the SATRAD curve at higher energies. The thinnest red curves are MIMI measurements for other selected periods of Enceladus orbit crossings: Julian days 48, 195, and 266 of 2005. A small peak at 0.03 MeV in the spectrum from day 48 is from a transient injection event. The Europa flux spectrum [*Cooper et al.*, 2001] is a composite of Galileo Orbiter data below 1 MeV from the Energetic Particle Detector [*Williams et al.*, 1992] and Pioneer-Voyager model data [*Divine and Garrett*, 1983] at higher energies up to 40 MeV. The Enceladus and Europa model spectra are extrapolated for surface interaction modelling as power laws to 1000 MeV from the lower energy measurements. Proton flux spectra are also shown as derived for cosmic ray protons (four dashed curves) in the outer supersonic heliosphere within the classical Kuiper Belt near 40 AU and in the outer heliospheric boundary regions [*Cooper et al.*, 2006] of the heliosheath and the local interstellar medium. The two 40-AU spectra are respectively for minimum [*Cooper et al.*, 2003] and maximum solar activity, the latter data being provided from previously unpublished Voyager data of co-author M. E. Hill.

Figure 4. Surface depth profiles in H_2O ice for time in years to accumulate chemically significant dosages of 60 gigarad (~ 110 eV per irradiated H_2O molecule) from total magnetospheric electron irradiation of Enceladus and Europa as compared to trans-neptunian objects. The two thin solid curves show the partial contributions of higher energy electrons at 1–10 MeV and 10–100 MeV to the Enceladus total irradiation at 10 keV to 1000 MeV, as compared to the total irradiation profile for Europa (dot-dot-dash curve). Comparative profiles (dashed curves) are also shown for cosmic ray proton irradiation of objects near 40 AU near solar minimum [*Cooper et al.*, 2003] and on highly eccentric orbits [*Cooper et al.*, 2006] passing through the heliosheath and into the local interstellar medium. Dosage time profiles are computed for isotropically incident fluxes onto flat surfaces from the flux spectra in Figure 3. The GEANT radiation transport code (http://wwwasd.web.cern.ch/wwwasd/geant/), as implemented in our earlier work [*Sturner et al.*, 2003; *Cooper et al.*, 2006], is used here for complete interactions of primary electrons, protons, and secondary

interaction products at energies above 10 keV from the flux spectra in Figure 3. Due to limitations on spatial step resolution in GEANT, the proton profiles have been extended to lower energies with stopping range and differential energy loss data of the Stopping and Range of Ions in Matter (SRIM) model [*Ziegler et al.*, 1985] (http://www.srim.org/) also used in the earlier work [*Cooper et al.*, 2001].

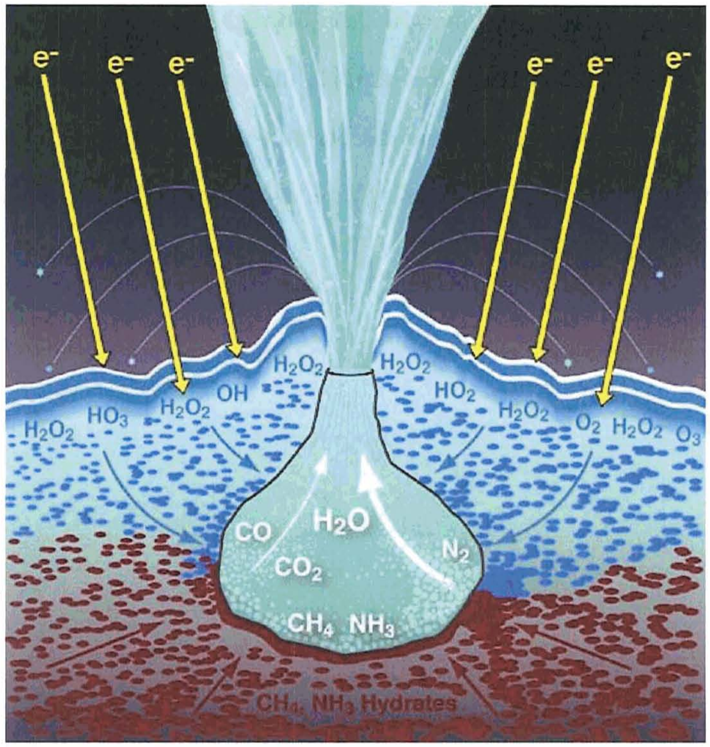

Figure 1. Illustration of radiolytic gas-driven cryovolvanism for potential subsurface liquid water reservoir near the surface of Enceladus. A continuous rain of energetic electrons (yellow arrows) drives radiolysis and saturates the upper ice surface with oxidants (blue), mostly H_2O_2 but with mix of other species. Transient plume activity ejects ice grains falling back to the surface (white ballistic curves) and depositing multiple layers of water frost (white) interspersed with oxidant concentrations accumulating during lower plume activity. Ice upwelling continuously supplies fresh "fuels" (red), e.g. hydrates of CH_4 and NH_4, from the deep interior. Exposure to increasing temperature within the ice margins of the fluid reservoir initiates sequences of exothermic reactions from H_2O_2 dissociation to fuel oxidation, resultant gas production, and fluid reservoir heating. Percolation of expanding hot gas bubbles from the margins into the incompressible water fluid becomes the driving force for upward movement (white arrows) of gas-saturated fluid to form the plumes. Interactions of lower (left side) or higher (right side) concentrations of oxidants and fuels produce correspondingly less or more gas.

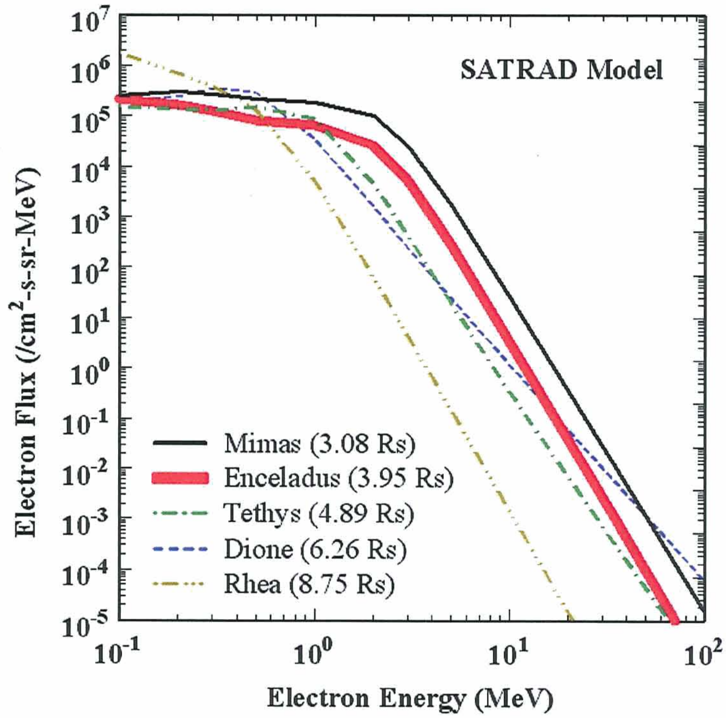

Figure 2. Representative differential flux spectra of Saturn magnetospheric electrons at the equatorial jovicentric orbits of the icy moons Mimas, Enceladus, Tethys, Dione, and Rhea as taken directly from the SATRAD model [*Garrett et al.*, 2005].

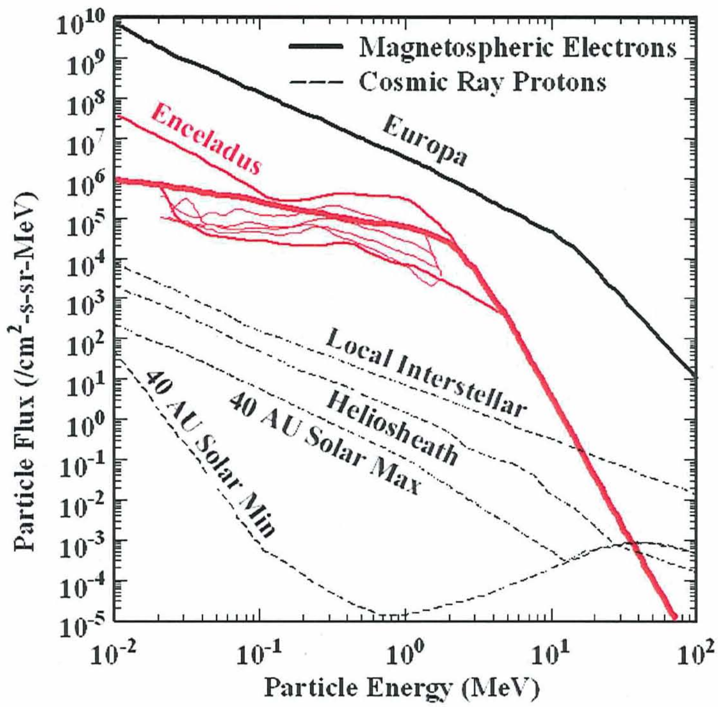

Figure 3. Differential flux spectra of energetic electrons (red curves) at Enceladus and Europa, respectively from the planetary magnetospheres of Saturn and Jupiter, and of cosmic ray protons (black curves) irradiating icy bodies within and beyond the heliosphere. The thickest solid Enceladus curve is from the SATRAD model. The two medium-thickness Enceladus curves are respectively upper and lower limits from Voyager and Cassini/MIMI electron data. The upper limit comes from Voyager measurements compiled by *Maurice et al.* [1996], and the lower limit is from Cassini electron flux measurements by the Magnetospheric Imaging Instrument (MIMI) experiment [*Krimigis et al.*, 2004] near the Jupiter-fixed longitude of this moon during the 9 March 2005 flyby. The limiting flux curves for Enceladus are extrapolated into the SATRAD curve at higher energies. The thinnest red curves are MIMI measurements for other selected periods of Enceladus orbit crossings: Julian days 48, 195, and 266 of 2005. A small peak at 0.03 MeV in the spectrum from day 48 is from a transient injection event. The Europa flux spectrum [*Cooper et al.*, 2001] is a composite of Galileo Orbiter data below 1 MeV from the Energetic Particle Detector

[*Williams et al.*, 1992] and Pioneer-Voyager model data [*Divine and Garrett*, 1983] at higher energies up to 40 MeV. The Enceladus and Europa model spectra are extrapolated for surface interaction modelling as power laws to 1000 MeV from the lower energy measurements. Proton flux spectra are also shown as derived for cosmic ray protons (four dashed curves) in the outer supersonic heliosphere within the classical Kuiper Belt near 40 AU and in the outer heliospheric boundary regions [*Cooper et al.*, 2006] of the heliosheath and the local interstellar medium. The two 40-AU spectra are respectively for minimum [*Cooper et al.*, 2003] and maximum solar activity, the latter data being provided from previously unpublished Voyager data of co-author M. E. Hill.

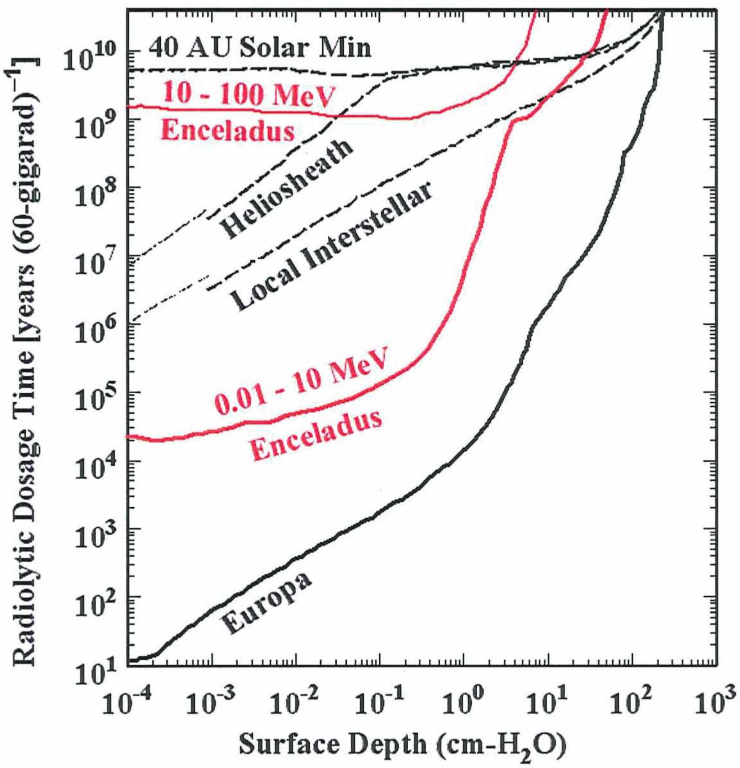

Figure 4. Surface depth profiles in H_2O ice for time in years to accumulate chemically significant dosages of 60 gigarad (~ 110 eV per irradiated H_2O molecule) from total magnetospheric electron irradiation of Enceladus and Europa as compared to trans-neptunian objects. The two thin solid curves show the partial contributions of higher energy electrons at 1–10 MeV and 10–100 MeV to the Enceladus total irradiation at 10 keV to 1000 MeV, as compared to the total irradiation profile for Europa (dot-dot-dash curve). Comparative profiles (dashed curves) are also shown for cosmic ray proton irradiation of objects near 40 AU near solar minimum [*Cooper et al.*, 2003] and on highly eccentric orbits [*Cooper et al.*, 2006] passing through the heliosheath and into the local interstellar medium. Dosage time profiles are computed for isotropically incident fluxes onto flat surfaces from the flux spectra in Figure 3. The GEANT radiation transport code (http://wwwasd.web.cern.ch/ wwwasd/geant/), as implemented in our earlier work [*Sturner et al.*, 2003; *Cooper et al.*,

2006], is used here for complete interactions of primary electrons, protons, and secondary interaction products at energies above 10 keV from the flux spectra in Figure 3. Due to limitations on spatial step resolution in GEANT, the proton profiles have been extended to lower energies with stopping range and differential energy loss data of the Stopping and Range of Ions in Matter (SRIM) model [*Ziegler et al.*, 1985] (http://www.srim.org/) also used in the earlier work [*Cooper et al.*, 2001].